Solar Physics (2006) 238: 207–217
DOI: 10.1007/s11207-006-0199-x

FIRST LIGHT OF THE NEAR-INFRARED NARROW-BAND TUNABLE BIREFRINGENT FILTER AT BIG BEAR SOLAR OBSERVATORY

WENDA CAO
Center for Solar-Terrestrial Research, New Jersey Institute of Technology, 323 Martin Luther King Blvd, Newark, NJ 07102, U.S.A.; Big Bear Solar Observatory, 40386 North Shore Lane, Big Bear City, CA 92314, U.S.A.
(e-mail: wcao@bbso.njit.edu)

KLAUS HARTKORN, JUN MA and YAN XU
Center for Solar-Terrestrial Research, New Jersey Institute of Technology, 323 Martin Luther King Blvd, Newark, NJ 07102, U.S.A.

and

TOM SPIROCK, HAIMIN WANG and PHILIP R. GOODE
Center for Solar-Terrestrial Research, New Jersey Institute of Technology, 323 Martin Luther King Blvd, Newark, NJ 07102, U.S.A.; Big Bear Solar Observatory, 40386 North Shore Lane, Big Bear City, CA 92314, U.S.A.

(Received 7 April 2006; accepted 9 August 2006; Published online 10 October 2006)

Abstract. We discuss a near-infrared (NIR) narrow-band tunable birefringent filter system newly developed by the Big Bear Solar Observatory (BBSO). This is one of the first narrow-bandpass NIR filter systems working at 1.56 μm which is used for the observation of the deepest solar photosphere. Four stages of calcite were used to obtain a bandpass of 2.5 Å along with a free spectral range (FSR) of 40 Å. Some unique techniques were implemented in the design, including liquid crystal variable retarders (LCVRs) to tune the bandpass in a range of $\pm$100 Å, a wide field configuration to provide up to 2° incident angle, and oil-free structure to make it more compact and handy. After performing calibration and characteristic evaluation at the Evans Facility of the National Solar Observatory at Sacramento Peak (NSO/SP), a series of high-resolution filtergrams and imaging polarimetry observations were carried out with the Dunn Solar Telescope of NSO/SP and the 65-cm telescope of BBSO, in conjunction with the high-order adaptive optics system and the Fabry–Pérot Interferometer (FPI). In this paper, we describe the optical design and discuss the calibration method. Preliminary observations show that it is capable of serving as either a stand-alone narrow-band filter for NIR filtergram observations or an order-sorting filter of a FPI applied to NIR two-dimensional imaging spectro-polarimetry.

1. Introduction

Benefiting from better seeing conditions, a larger Zeeman line splitting, weaker instrumental polarization, lower contamination by stray light, and lower requirements for the adaptive optics system, near-infrared (NIR) observations have proven to be a powerful and promising tool to probe small-scale solar magnetic features (Kopp and Rabin, 1992; Lin, 1995; Livingston, 2002; Penn *et al.*, 2003a,b,c). However, until now, almost all universal birefringent filters (UBF) on duty have been built to operate

in the visible wavelengths. Therefore, only few reports regarding NIR narrow-band filter imaging observations of solar features exist (Tomczyk *et al.*, 2004).

Big Bear Solar Observatory (BBSO) is developing the InfraRed Imaging Magnetograph system (IRIM), which is a two-dimensional imaging spectro-polarimeter working in the NIR. This system will be used at the 65-cm telescope of BBSO, and subsequently at the 1.6-m New Solar Telescope under development at BBSO, as well as the future Advanced Technology Solar Telescope of NSO. It consists of an interference pre-filter, a birefringent filter, a FPI, and a polarization analyzer. Acting as the order-sorting filter for the FPI, the NIR narrow-band tunable birefringent filter system has been designed and implemented by BBSO/NJIT, in collaboration with the Cambridge Research & Instrumentation Inc. In order to match the transmission profiles of the interference pre-filter and the FPI, four stages of calcite are employed to acquire a 2.5 Å bandpass over a diameter of 37 mm. Liquid crystal variable retarders (LCVRs) are first utilized to tune the bandpass over a range of ± 100 Å. In November 2004, the calibration and characteristic evaluation were performed with an auto-collimation infrared spectrograph set up at the Evans Facility of NSO/SP. Shortly after that, high spatial resolution NIR filtergram observations were obtained with the Dunn Solar Telescope (DST) of NSO/SP, utilizing the high-order adaptive optics system. In July 2005, diffraction-limited polarimetry observations were successfully carried out with the IRIM at BBSO. In this paper, we present the optical design and the calibration, as well as some preliminary observational results.

2. Optical Design and Implementation

The spectral line Fe I 15648.5 Å (e^7D_1-$3d^64s5p^7D_1^0$), a normal Zeeman triplet, with a Landé factor of 3 has already proved to be one of the most important diagnostic tools for understanding the structure of the deep photosphere and its vector magnetic field. Combined with its adjacent Fe I 15652.9 Å ($f^7D_5 - (9/2)[7/2]_4^0$, $g_{\rm eff} = 1.53$) spectral line, a magnetic field strength as low as 100 G can be measured using the line pair ratio method (Stenflo, 1973; Rabin, 1992). The first objective of the IRIM is to carry out high angular resolution, high cadence, high spectral resolving power, and high magnetic sensitivity imaging spectroscopy and/or polarimetry from these two lines. The characteristic evaluation of the FPI for IRIM have been performed by Cao *et al.* (2004), with a NIR He–Ne laser and a spectrograph, respectively. It will provide 0.1 Å bandpass with a free spectral range (FSR) of 5.5 Å at a wavelength of 1.565 μm. Serving as the order-sorting filter of the FPI, the design of the NIR birefringent filter faces many challenges in side-lobe suppression, high throughput, flexible tunability, and stability.

2.1. Optical Layout

The optical design of the birefringent filter was described in detail by Wang *et al.* (2001). As shown in Figure 1, it is composed of four birefringent crystal

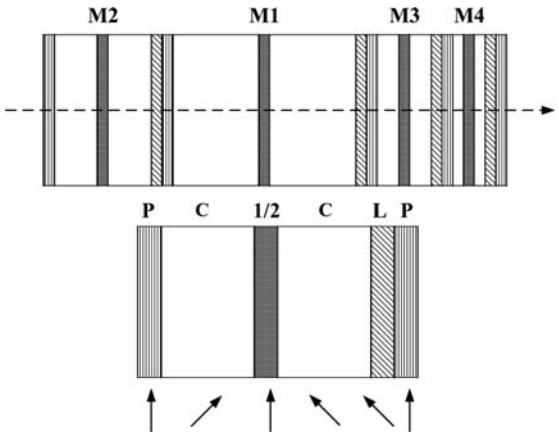

Figure 1. Optical diagram of the NIR narrow-band tunable birefringent filter. The upper half of the figure shows the scheme of four birefringent modules marked by M_1, M_2, M_3, and M_4. The lower half shows the detailed optical configuration of a single tunable wide field module. *P*: polarizer; *C*: Calcite; 1/2: half waveplate; *L*: LCVR; *arrows* represent the direction of optical axis for each optical element.

modules with a aperture of 37 mm × 37 mm. In each module, an octagonal calcite is sandwiched between two parallel linear polarizers. In order to reduce the retardation error caused by non-normal incident light on the field of view (FOV), a wide field configuration is used in each module: each calcite is split into two equal parts with their optical axes crossed, and the two halves sandwich a half waveplate with the optical axis at 45° to them. Tuning of the filter is accomplished by adding a LCVR to each module with its optical axis parallel to the attached calcite crystal. By changing the voltage imposed on LCVR, one can tune the bandpass of each module rapidly. A new oil-free internal structure is used in the design: all optical elements are agglutinated with a specific epoxy material in a thermally controlled housing. This unique design makes the system more compact and handy, while avoiding many drawbacks of the traditional UBF, especially in internal oil leakage and maintenance. The thickest module is located in the middle of the filter for better thermal control.

2.2. THICKNESS OF THE CALCITE STAGES

In compliance to the principle of a traditional UBF, the transmission τ at specific wavelength λ is given by

$$\tau = \cos^2\left(\pi\frac{\mu d_1}{\lambda}\right)\cos^2\left(\pi\frac{\mu d_2}{\lambda}\right)\cos^2\left(\pi\frac{\mu d_3}{\lambda}\right)\cos^2\left(\pi\frac{\mu d_4}{\lambda}\right), \quad (1)$$

where d_i is the calcite thickness of ith module ($i = 1, 2, 3, 4$), $\mu(\lambda, T)$ is the birefringent index relevant to the wavelength and temperature. Assuming $d_1 = 2d_2 = 4d_3 = 8d_4$, the four transmission profiles are coupled to provide a

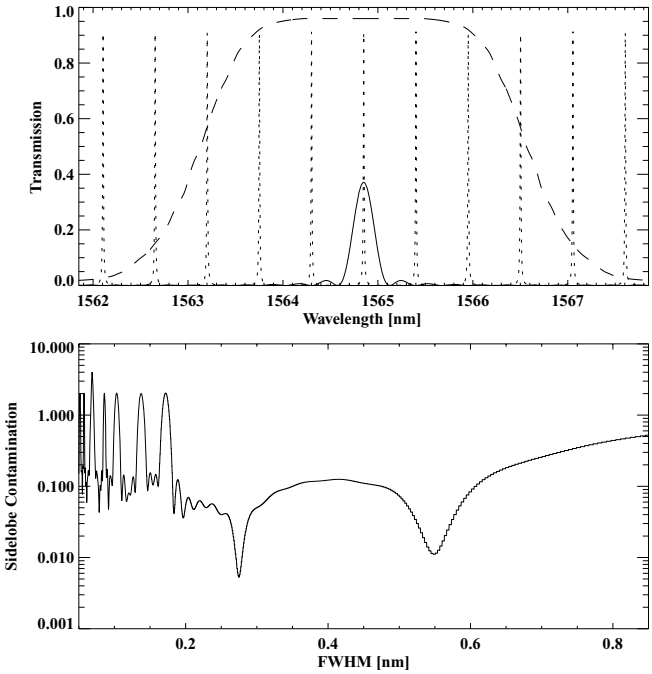

Figure 2. (*Top*) Transmission profiles of the birefringent filter (*solid curve*), the FPI (*dotted curve*), and the interference filter (*dashed curve*). (*Bottom*) Contamination from sidebands as a logarithmic function of FWHM of the birefringent filter bandpass. A contamination as low as 0.53% can be obtained with a FWHM approaching 2.744 Å.

comparatively narrow bandpass with a suitable FSR (spectral span between the adjacent bandpass peaks). The full width at half maximum (FWHM) of the transmission bandpass will be determined by the thickness of the thickest module d_1, while FSR by the thickness of the thinnest d_4.

Figure 2 shows the transmission profiles of a birefringent filter (solid curve), a FPI (dotted curve), and an interference filter (dashed curve). For high spectral purity of the IRIM system, it is essential to match these transmission profiles to each other. As illustrated in Figure 2, the profile of the birefringent filter has a main transmission band with several side bands. The contamination contributed by the side bands can reach over 8% due to a mismatching of the birefringent filter and the FPI. A simulation was performed to understand the degree of contamination caused by the side-lobes for the different FWHM of the birefringent filter. As shown in Figure 2, a contamination as low as 0.53% can be obtained with a FWHM approaching 2.744 Å. This value is taken as reference for determining d_1.

When the FWHM of the first module is set to be 2.5 Å, the fourth module would have a FWHM of 20 Å and the corresponding FSR is 40 Å. By using a three-cavity interference filter with a FWHM of 40 Å, the adjacent main band is blocked completely.

2.3. THE LIQUID CRYSTAL TUNING ELEMENT

Theoretically, there are a number of ways to tune the transmission wavelength. Polarizer rotation is the most widely used method in traditional UBFs (Beckers, Dickson, and Joyce, 1975). In this configuration, each module is equipped with an achromatic quarter waveplate with its optical axis at 45° to the axis of the crystal. Tuning is implemented by rotating the polarizer following the quarter waveplate. In recent years, progress in the swift electro-optical modulators, especially the LCVR, have made it possible to use them instead of a rotating waveplate.

As shown in Figure 1, each module has an individual LCVR tuning element, and the relevant transmission can be expressed as

$$\tau_i = \cos^2\left[\left(\frac{\mu d_i}{\lambda} + \delta_i\right)\pi\right] = \cos^2[(\sigma_i + \delta_i)\pi], \tag{2}$$

where δ_i is the retardance of the LCVR in its ith stage. The retardance is controlled by the drive voltage imposed on it. Up to 14.0 V voltage is digitalized into 12-bit corresponding to the drive range of $0-4096$ counts. A RS-232 interface is used for communication between the host PC and LCVR drive electronics. One command is processed in approximately 1 ms, and the LCVR takes up to 100 ms to respond, depending on the levels of the previous drive and new drive. Since the electro-optic response of the LCVR shows obvious nonlinearity, the filter must be calibrated to determine the correct voltages at different wavelengths.

2.4. THERMAL CONTROLLER

In Equation (2), μ, d_i and δ_i are very sensitive to the variation of the ambient temperature. A thermal controller system is used to maintain a stable temperature of 32.0 °C. This system consists of a CN76000 Microprocessor-Based Temperature/Process unit from Omega Engineering Inc., four 100Ω Pt RTD-850 temperature sensors embedded into the insulating housing to monitor the temperature variation at different positions, and an auto-tuned PID single-input/single-output controller to provide 0.1 °C resolution, in conjunction with a flexible silicon rubber fiberglass insulated heater.

3. Calibration and Evaluation

In order to tune the transmission bandpass of the filter exactly to the desired spectral line, it is essential to calibrate the LCVRs by utilizing a higher resolution spectrograph. In particular, the important parameters such as LCVR voltages or drive counts corresponding to specific solar Fraunhofer line have to be determined.

3.1. INSTRUMENTATION

The 12-inch coelostat telescope of the Evans Facility of NSO/SP was used to feed the solar beam for calibration. The system is a horizontal coelostat illuminating a Fraunhofer Doublet with an aperture of 30 cm and a focal length of 10.75 m, which is determined by measuring the diameter of the solar image in prime focus. A set of relay optics is designed to illuminate the birefringent filter system in a collimated mount. The beam through the filter is collimated to better than a f-number of 300. An auto-collimation infrared spectrograph is tentatively set up by using a large and adjustable slit, a coated singlet with a focal length of 1.7 m and an aperture of 100 mm, and a grating with 79 grooves/mm blazed at an angle of $63^\circ 26'$. The flexible setup allows us to obtain the desired spectral scale by using different orders. The data are recorded by a 1024×1024 pixel, 14-bit HgCdTe CMOS focal plane array camera (Cao *et al.*, 2005). For calibration, the 15th order was utilized to obtain a high enough spectral resolution. At this order, the spectral dispersion is 0.0786 Å per pixel.

3.2. APPROACH AND RESULT

Since all four modules have been agglutinated together, more difficulties have to be overcome compared to the individual module calibration. Using the above spectrograph, the transmission image sequences are acquired by scanning the drive voltage count from 0 to 4096 for each module. To improve the signal-to-noise ratio, each image in sequence is integrated along the slit direction to form a transmission profile for a specific drive voltage. A calibration image can be composed from these transmission profiles under different voltage drives. Figure 3 illustrates the

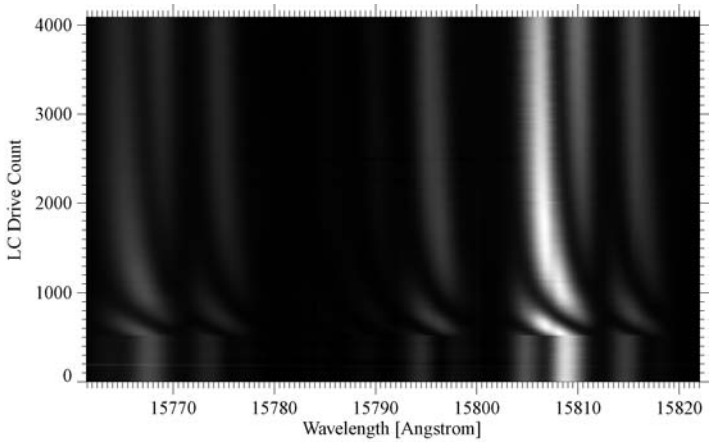

Figure 3. The transmission of the thickest module M_1 as a function of drive voltage V and wavelength λ. The retardance of LCVR does not have any response in the range of 0 – 500 counts. The *horizontal slices* along the x-axis present the transmission profiles under different drive voltage. The *vertical slices* along the y-axis present the calibration curves as transmission vs. drive voltage under 32.0 °C.

calibration image of M_1 as a function of the drive voltage V and wavelength λ. Due to the transmission mismatching of M_2, M_3, and M_4, the calibration image shows several similar patterns with different transmission intensity. As expressed in Equation (2), the retardance δ of LCVR in each module is used to tune the central transmission. Assuming λ_1 to be the wavelength corresponding to the maximum transmission and λ_0 to be the objective wavelength,

$$\left(\frac{\mu d}{\lambda_1} + \delta'\right)\pi = \left(\frac{\mu d}{\lambda_0} + \delta''\right)\pi \tag{3}$$

should be sustained following Equation (2). If $\triangle\lambda = \lambda_1 - \lambda_0 \ll \lambda_1 \cdot \lambda_0$, we have

$$\frac{d\delta(V)}{dV} \cdot \triangle V = \frac{\triangle\lambda}{p}, \tag{4}$$

where the FSR $p = -\lambda^2/\mu d$. $\delta(V)$ usually shows a hyperbolic function of V, and $d\delta(V)/dV$ can be derived from the calibration curves in Figure 3. So, the correct drive voltage $V_0 = \triangle V - V_1$ can be determined at λ_0.

We performed this analysis for all four modules to obtain the corresponding drive voltage values at any wavelength desired. The matrix $M[V_i(\lambda)]$ has been created and stored in the host PC for the future wavelength tuning. Figure 4 shows

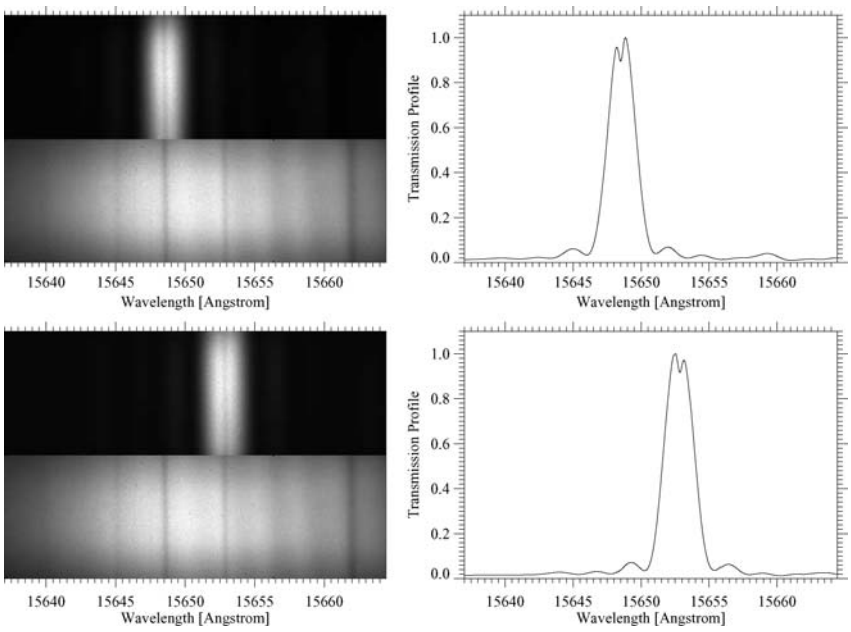

Figure 4. The calibration results and transmission profiles when tuned to Fe I 15648.5 Å and Fe I 15652.9 Å spectral lines. (*Left panel*) The transmission bandpass of the spectrograph including or excluding the filter system in the calibration optical path. (*Right panel*) The corresponding transmission profiles. The concave centering at the peak shows the core of the spectral line.

the calibration results when tuned to the Fe I 15648.5 Å and Fe I 15652.9 Å spectral lines. The symmetrical profiles imply that the transmissions of the four modules are well matched. Meanwhile, some parameters are measured and given as follows by virtue of the transmission profile: FWHM $= 2.46 \pm 0.05$ Å; FSR $= 39.7 \pm 0.5$ Å; and the peak transmission is about 15.9% for the unpolarized beam.

4. Observations

We present two examples in many scientific applications of this filter system. On December 1 and 2, 2004, high-cadence, high-resolution filtergrams of solar active region NOAA AR 10707 were obtained simultaneously in the NIR continuum and the visible with the DST of NSO/SP. In 2-days' observations, the NIR filter was tuned to 15657.0 Å to collect images in a line-free NIR continuum window. The exposure time was 13 ms, and 10 NIR frames were obtained every second. Figure 5 shows a NIR snapshot of NOAA AR 10707. The spatial resolution was

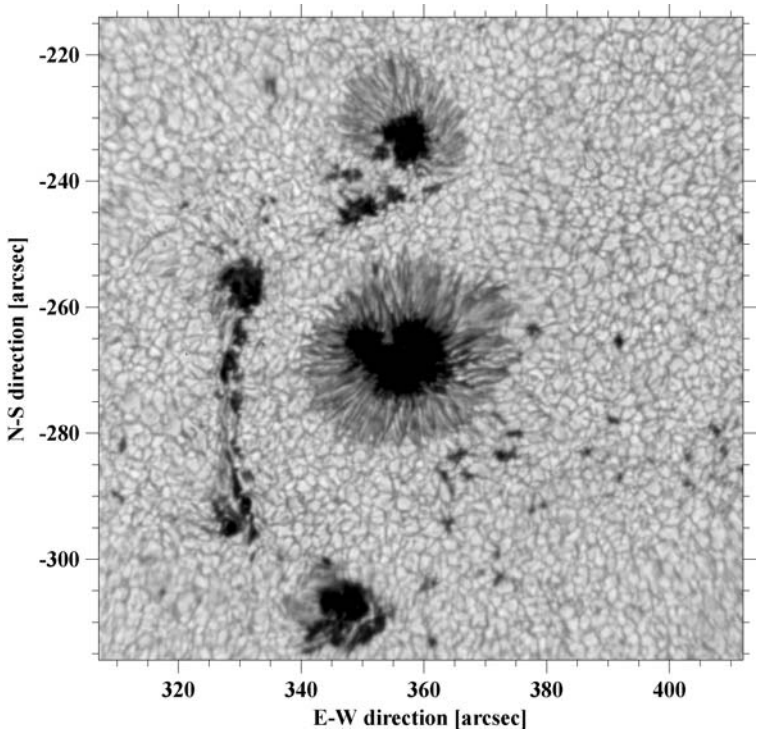

Figure 5. NIR snapshot of NOAA AR 10707 on December 1, 2004, at 17:50 UT. The filter was tuned to 15657.0 Å with a bandpass of 2.5 Å. A number of small-scale features are seen clearly in a FOV of 120 arcsec × 120 arcsec. The image scale is about 0.12 arcsec/pixel.

close to the diffraction limit of the 76-cm aperture DST with assistance of the high order adaptive optics system. Since the opacity reaches its minimum at around 1.6 μm due to H^- absorption, these data provide crucial information about the deepest layer of the solar atmosphere. A number of dynamic behaviors and the structure of small-scale features were tracked and investigated. After comparing the NIR and visible faculae observations, Xu *et al.* (2005) found no evidence for the existence of the so-called dark faculae. More scientific results concerning dynamic behavior of small-scale structures will be addressed in forthcoming papers.

On July 1, 2005, diffraction-limited polarimetric observations were successfully carried out with the IRIM at BBSO (Cao *et al.*, 2006). The birefringent filter was first combined with the FPI and polarization analyzer for measuring the solar longitudinal magnetic field by using the Fe I 15648.5 Å line. Figure 6 presents an example of the IRIM results. From a comparison with MDI's magnetograms, it is

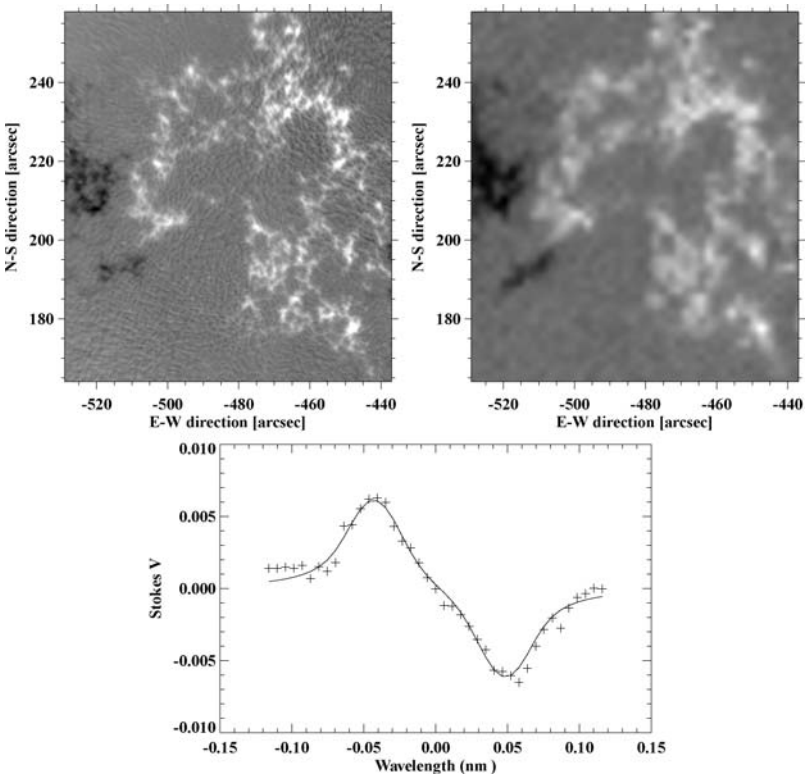

Figure 6. Magnetograms of NOAA AR 10781 obtained by IRIM at 16:02 UT (*left*) and MDI at 16:00 UT (*right*). (*Bottom panel*) Stokes V profile and its fitting of an interesting small-scale magnetic structure. The fitted intrinsic field strength is 482 G with a filling factor 49.3%, and the corresponding true magnetic flux is 2.04×10^{17} Mx on an area of 206 km $\times$ 206 km.

obvious that the IRIM has approached the diffraction limit of the BBSO's 65-cm telescope with a high magnetic sensitivity. Also, Stokes V profiles for all resolution elements are extracted from magnetograms obtained by tuning the Fabry–Pérot etalon from -1.16 Å ($blue\ wing$) to $+1.16$ Å ($red\ wing$) from the line center in steps of 0.058 Å. The bottom panel shows the Stokes V profile and its fitting for a selected point in a newly discovered magnetic structure with the IRIM system: the elongated channel structure along the intergranular lanes. Both the true magnetic field strength and the filling factor were derived from the fitting curve. The details were discussed in Cao *et al.* (2006).

5. Summary

A NIR narrow-band tunable birefringent filter system has been fabricated, calibrated, and is successfully running at BBSO. The unique LCVRs are used to tune the bandpass within a range of ± 100 Å in the NIR. This is one of the first NIR narrow-band filter systems used for probing the deepest solar photosphere at the 1.6 μm opacity minimum. In addition, as a part of IRIM, it acts as a pre-filter with a bandpass of 2.5 Å at the Fe I 15648.5 Å and Fe I 15652.9 Å spectral lines. The achieved photometric and polarimetric data have demonstrated the stability, reliability, and flexibility in the above issues. We are in the process of further upgrading the IRIM system. Accordingly, a new NIR universal birefringent filter system is under consideration to extend the tuning to cover the wavelength range from 1 to 1.7 μm.

Acknowledgements

We would like to express special thanks to the Cambridge Research & Instrumentation Inc. for the fabrication of this filter system. Thanks go to the staff of the Evans Facility and the DST of NSO/SP for their immeasurable support in calibration and observation. This work is supported by NSO subcontract through NSF ATST project and NSF under grant ATM-0320540. We gratefully acknowledge the referee for valuable comments.

References

Beckers, M.J., Dickson, L., and Joyce, R.S.: 1975, *Appl. Optics* **14**, 2061.

Cao, W., Denker, C., Wang, H., Ma, J., Qu, M., Wang, J., and Goode, P.R.: 2004, *Proc. SPIE* **5171**, 307.

Cao, W., Xu, Y., Denker, C., and Wang, H.: 2005, *Proc. SPIE* **5881**, 245.

Cao, W., Jing, J., Ma, J., Xu, Y., Wang, H., and Goode, P.R.: 2006, *Publ. Astron. Soc. Pacific* **118**, 838.

Kopp, G. and Rabin, D.: 1992, *Solar Phys.* **141**, 253.

Lin, H.: 1995, *Astrophys. J.* **446**, 421.
Livingston, W.: 2002, *Solar Phys.* **207**, 41.
Penn, M.J., Cao, W., Walton, S.R., Chapman, G.A., and Livingston, W.: 2003a, *Astrophys. J.* **590**, L119.
Penn, M.J., Walton, S.R., Chapman, G.A., Ceja, J.A., and Plick, W.: 2003b, *Solar Phys.* **213**, 55.
Penn, M.J., Cao, W., Walton, S.R., Chapman, G.A., and Livingston, W.: 2003c, *Solar Phys.* **215**, 87.
Rabin, D.: 1992, *Astrophys. J.* **391**, 832.
Stenflo, J.O.: 1973, *Solar Phys.* **32**, 41.
Tomczyk, S., Card, G.L., Darnell, T., Elmore, D.F., Casini, R., Judge, P.G., and Burkepile, J.: 2004, *AAS* **204**, 20.02.
Wang, J., Wang, H., Spirock, T.J., Lee, C.Y., Ravindra, N.M., Ma, J., Goode, P.R., and Denker, C.: 2001, *Opt. Eng.* **40**, 1016.
Xu, Y., Cao, W., Ma, J., Hartkorn, K., Jing, J., Denker, C., and Wang, H.: 2005, *Astrophys. J.* **628**, L167.